Observation of the $\tilde{A}-\tilde{X}$ Electronic Transition of the Isomers and Conformers of Pentyl Peroxy Radical Using Cavity Ringdown Spectroscopy

Erin N. Sharp, Patrick Rupper, and Terry A. Miller*

Laser Spectroscopy Facility, Department of Chemistry, The Ohio State University, 120 W. 18th Avenue, Columbus, Ohio 43210

Received: September 18, 2007; In Final Form: November 15, 2007

Cavity ringdown spectra of the $\tilde{A}-\tilde{X}$ electronic transition of all eight isomers of the pentyl peroxy radical are reported. Using the corresponding assignments from previously studied smaller alkyl peroxy radicals, assignments of origin bands are made for the pentyl peroxy isomers including some conformer-specific assignments for bands of a given isomer. Ab initio calculations also were performed to aid in the spectral assignments for neopentyl, *t*-butyl, and *t*-pentyl peroxies. In addition to the origins, vibrational bands have also been assigned for some species. Using the analyzed spectra, the relative reactivity of the primary, secondary, and tertiary hydrogen atoms in isopentane could be determined semiquantitatively.

1. Introduction

The formation of alkyl peroxy radicals (RO_2) is a crucial step in both the low-temperature combustion ($T < 700$ K) of hydrocarbons[1,2] and in atmospheric hydrocarbon oxidation.[3−5] The mechanism of low-temperature combustion[6,7] begins with the abstraction of a hydrogen atom from the hydrocarbon fuel (RH) by a hydroxyl radical (OH) to form an alkyl radical (R). This alkyl radical then reacts with molecular oxygen to form an alkyl peroxy radical (RO_2).

$$R + O_2 \leftrightarrows RO_2 \tag{1}$$

Production of RO_2 maintains the forward rate of low-temperature combustion as it is involved in a chain-branching sequence of reactions that ultimately leads to the production of OH radicals, which speed up the overall rate combustion. The competition between the alkyl radical's reaction with O_2 to form a peroxy radical and its self-reaction, or reaction with other hydrocarbon-containing species, to form larger hydrocarbons is critical to the amount of soot produced from combustion.[8] In addition, from 550 to 700 K, a negative temperature coefficient (NTC) has been observed[9] in the rate of combustion of hydrocarbons, which is largely attributed to the RO_2 formation step. As temperature increases in this NTC regime, the equilibrium of eq 1 lies toward the reactants, and with increased concentrations of R and O_2 as well as slightly higher temperatures, higher activation energy reaction pathways of $R + O_2$ can compete with the formation of RO_2.[10] The most typical of these is the abstraction of a hydrogen atom (H) from R to form an alkene $+ HO_2$. When this alternate reaction becomes competitive, the supply of alkyl peroxy radicals, necessary for chain-branching to occur, is depleted and the forward rate of combustion slows. Hence, even with increasing the temperature between 550 and 700 K, the rate of combustion decreases, giving rise to this NTC behavior.

Previous kinetic studies of the pentyl peroxy radicals ($C_5H_{11}O_2$) have centered often on neopentyl peroxy radical[11−13] (see Figure 1), due to two characteristics unique to its structure. First, all of the C−H bonds in neopentane are equivalent, so only one alkyl radical isomer is possible, and hence, only one alkyl peroxy radical isomer is possible, making the chemistry much less complicated than starting with *n*-pentane or isopentane. Second, and of particular interest to combustion chemistry, neopentyl radical has the radical site connected to a quaternary carbon, making the formation of a C_5 alkene $+ HO_2$ from the alternate pathway of $R + O_2$, mentioned above, structurally impossible. Therefore, this eliminates one mechanistic alternative, which can hinder the forward rate of low-temperature combustion. Ergo, studies on the combustion of neopentane have instead been able to shed some light on the later steps of the overall mechanism that were not possible to isolate in other molecules studied.

The oxidation of hydrocarbons in the atmosphere is initiated by, again, a reaction with OH radicals to form alkyl radicals. Then R rapidly reacts with O_2 in a three-body process to form RO_2. In polluted atmospheres, these alkyl peroxy radicals can react with nitric oxide (NO) according to the following equation:

$$RO_2 + NO \rightarrow NO_2 + RO \tag{2}$$

This reaction upsets the normal balance of NO and NO_2 in the troposphere, which is maintained by the reaction scheme:[6]

$$NO_2 + h\nu(\lambda = 430\ \text{nm}) \rightarrow NO + O(^3P) \tag{3}$$

$$O(^3P) + O_2 + M \rightarrow O_3 + M \tag{4}$$

$$O_3 + NO \rightarrow NO_2 + O_2 \tag{5}$$

By themselves, eqs 3−5 yield no net production of ozone (O_3), but the presence of alkyl peroxy radicals in the troposphere can competitively deplete the amount of NO (see eq 2) and thereby reduce the amount of O_3 destroyed in eq 5. It is estimated that the atmospheric chemistry of peroxy radicals is responsible for ≈90% of the ozone present in the troposphere.[14]

Given that peroxy radicals are involved in many complex reaction mechanisms, whose rates can be greatly affected by the structural form of the peroxy, it is very desirable to observe

* To whom correspondence should be addressed.

10.1021/jp077521u CCC: $40.75
Published on Web 01/23/2008

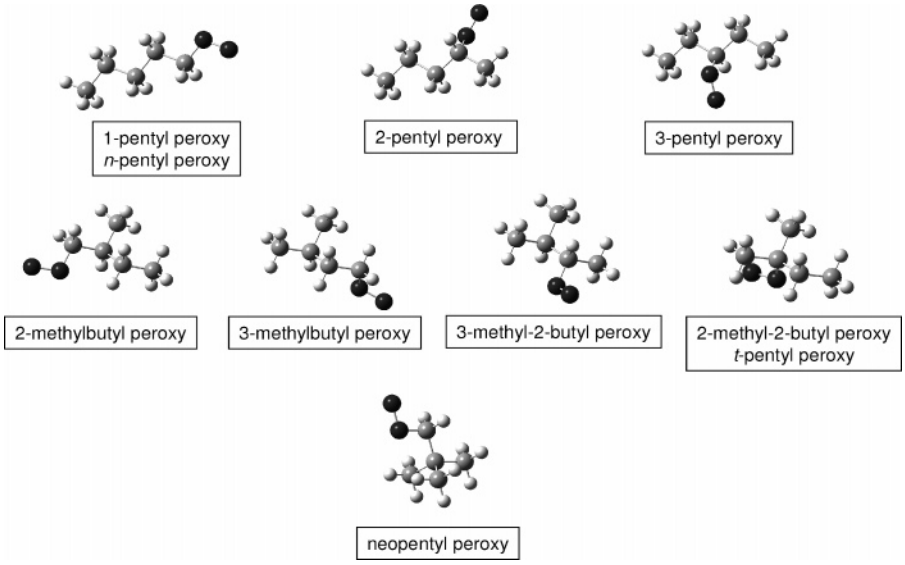

Figure 1. Eight isomers of pentyl peroxy radical. They are separated into three different groups based on the isomer of the pentyl backbone in each peroxy: three isomers have the *n*-pentyl backbone, four have the isopentyl backbone, and one has the neopentyl backbone.

and analyze peroxy radical spectra to establish the foundation for spectroscopic diagnostics of different isomers and conformers of a given peroxy radical. Previous spectroscopic studies of pentyl peroxy radicals ($C_5H_{11}O_2$), namely *n*-pentyl[15] and neopentyl[13,16−18] peroxies, have centered around the strong $\tilde{B}-\tilde{X}$ electronic transition located in the UV around 240 nm, which has proven to be a good diagnostic for measuring kinetic properties of the peroxy radical. However, the $\tilde{B}$ electronic state is dissociative,[19] making the $\tilde{B}-\tilde{X}$ transition broad and structureless. In addition, this transition overlaps for many of the alkyl peroxy radicals in the gas phase,[20] making identification of a particular peroxy radical very difficult. More recently, therefore, spectroscopic studies have shifted their focus to the much weaker $\tilde{A}-\tilde{X}$ transition, located in the near-infrared (NIR). NIR cavity ringdown spectroscopic (CRDS) studies of methyl,[21] ethyl,[21,22] propyl,[23] and butyl[24] peroxy radicals have proven that the $\tilde{A}-\tilde{X}$ electronic transition has well-defined structure, making it a good diagnostic to distinguish between not only different alkyl peroxy radicals (RO_2 vs $R'O_2$) but also between isomers and conformers of the same RO_2.

In the following, we report the extension of our NIR CRDS studies to $C_5H_{11}O_2$. As was already observed in going from ethyl to propyl to butyl peroxy, increasing the number of carbons in the R group increases the structural diversity of RO_2. Various isomers and conformers can be formed depending on the branching of the hydrocarbon moiety and the orientation of the oxygens with respect to the rest of the molecule. We present, herein, the spectra of all eight pentyl peroxy isomers (structures presented in Figure 1), and make some suggested conformeric assignments in each isomer's origin spectrum using the assignments of 1- and 2-propyl peroxy as a guide,[25] which were based on extensive quantum-chemical calculations. Since there are approximately 170 stable conformers in total for the 8 isomers, complete assignment of specific bands to all conformers is not possible. However, propyl peroxy assignments were already extended to butyl peroxy radical,[24] and the features in all four butyl peroxy isomers' spectra were relatively well-explained by this extrapolation. Therefore, the groundwork already exists for making the corresponding isomeric and conformeric assignments in $C_5H_{11}O_2$, rather than needing to rely on ab initio calculations to make predictions. This is especially important since current ab initio methods are somewhat unreliable for these large open shell systems.

2. Experimental Section

2.1. NIR CRDS Apparatus. The cavity ringdown setup has been described in detail previously[22] and so will only be briefly discussed here. The second harmonic light from a Nd:YAG laser (20 Hz Quanta-Ray PRO-270) pumped a dye laser system (Spectra Physics SIRAH) equipped with DCM, Rhodamine B, Rhodamine 101, SulfuRhodamine B, and Pyrromethene 597 dyes to reach the region of 644−572 nm, with pulse energies of 50−100 mJ and a laser line width of ≈0.03 cm^{-1} (fwhm). The output of the dye laser was focused into a single pass high-pressure Raman cell filled with molecular hydrogen, generating 2nd Stokes radiation in the 1.39−1.09 μm (7194−9174 cm^{-1}) region. This NIR light, with pulse energies of 1−2 mJ, was then directed into the ringdown cavity and used to probe the pentyl peroxy radicals from their ground electronic $\tilde{X}$ state into their first excited electronic $\tilde{A}$ state. The ringdown cavity was formed by two highly reflective mirrors ($R \geq 99.99\%$, Los Gatos Research), and mirror sets centered at 1.064, 1.2, and 1.3 μm were used to obtain continuous coverage of the investigated spectral region. A Thorlabs InGaAs (PDA400) photodiode was used to detect the outcoming radiation, and its output was recorded by a 12 bit digitizing card (Measurement Computing) for further analysis. For obtaining CRDS spectra, the signals of twenty consecutive laser shots were averaged at each dye-laser frequency point. Spectra were recorded with ≈0.5 cm^{-1} laser step size typically and were calibrated using water absorption lines published in the HITRAN database.[26]

To initiate the chemistry necessary for producing $C_5H_{11}O_2$ radicals, the radiation at 193 nm from a photolysis excimer laser (LPX120i, Lambda Physik) was focused by a cylindrical and a spherical lens to a rectangular shape (13×0.5 cm^2). Five microseconds before the probe beam (NIR light) entered the ringdown cavity, the excimer light passed once through the ringdown cell via UV-grade quartz windows at the central part of the cavity. At each dye-laser frequency point, a ringdown time was acquired with the photolysis excimer laser on and off, as taking the difference between these two traces removes

background absorptions and leaves only the spectra of molecules produced from photolysis.

2.2. Production of Pentyl Peroxy Radicals. Pentyl peroxy radicals were produced in the CRDS cell via a three-body reaction involving pentyl radicals (C_5H_{11}), nitrogen (N_2), and oxygen (O_2). C_5H_{11} radicals were produced using two methods: direct photolysis of pentyl bromides ($C_5H_{11}Br$) and hydrogen abstraction from *n*-pentane/isopentane/neopentane (C_5H_{12}) by a chlorine atom, produced from the photolysis of oxalyl chloride ($(COCl)_2$).

The direct photolysis of alkyl bromides has been used as the initiation step previously to produce both propyl[23] and butyl[24] peroxy radicals. Using 193 nm light from the excimer laser, the carbon-bromine bond of the pentyl bromides was broken to produce C_5H_{11}, which then reacted with O_2, also present in the cell, to form pentyl peroxy radicals via a three-body collision involving N_2. For each pentyl peroxy radical isomer, the corresponding pentyl bromide was used to initiate production, making this method isomer-specific (i.e., for each pentyl bromide, only one pentyl peroxy isomer was observed to be produced). These pentyl bromides are liquids at room temperature, so N_2 was bubbled through the liquid precursor to carry it into the ringdown cell. Before entering the cell, O_2 was mixed into the reactant mixture, so that as soon as pentyl radicals were produced by photolysis, the peroxy radical formation step quickly proceeded before other radical−radical reactions could occur. Typical experimental concentrations for this method were $[C_5H_{11}Br] \approx 1-2$ Torr, $[O_2] = 100$ Torr, and $[N_2] = 150$ Torr. With energies of 150 mJ/pulse from the photolysis laser, this gives a photolysis flux of 193 nm photons passing through the ringdown cell of 2.2×10^{16} cm^{-2}. Using an estimated absorption cross section for pentyl bromide at 193 nm of $\sigma \approx 5 \times 10^{-19}$ cm^2/molecule (same as that for butyl bromide[24] since the addition of one CH_2 group will not likely change the cross section significantly), the photolysis flux and the $[C_5H_{11}Br]$ from above, the number of C_5H_{11} radicals produced from this method is $\approx 7 \times 10^{14}$ cm^{-3}.

The alternate method of pentyl peroxy radical production involves the abstraction of a hydrogen atom (H) from a stable pentane molecule by a chlorine atom (Cl). This initiation step has also been used previously to produce ethyl,[22] propyl,[23] and butyl[24] peroxy radicals. Photolyzing oxalyl chloride ($(COCl)_2$) at 193 nm efficiently produces two chlorine atoms per excimer photon by breaking the carbon-chlorine bonds in the molecule.[27]

$$(COCl)_2 \xrightarrow{193\ nm} 2Cl + 2CO \qquad (6)$$

These chlorine atoms react with C_5H_{12} by abstracting an H to produce C_5H_{11} radicals. As with the direct photolysis method, C_5H_{11} then reacted with O_2 to form $C_5H_{11}O_2$ radicals via a three-body collision with N_2. Unlike with the pentyl bromides, however, these pentane precursors are not isomer-specific predecessors to pentyl peroxy radicals, except for neopentane which can only produce one unique peroxy isomer, namely neopentyl peroxy. Figure 2 illustrates this production method for isopentane, whereby abstracting the H from four different positions in the molecule results in four unique isomers of "isopentyl peroxy". Isopentane was used to produce 2-methylbutyl peroxy, 3-methylbutyl peroxy, 3-methyl-2-butyl peroxy, and 2-methyl-2-butyl peroxy (*t*-pentyl peroxy); *n*-pentane was used to produce 1-pentyl peroxy (*n*-pentyl peroxy), 2-pentyl peroxy, and 3-pentyl peroxy; neopentane was used to produce neopentyl peroxy. Isopentane and *n*-pentane are liquids are room temperature, so as was the case with the pentyl bromides, N_2 was bubbled through the liquid precursor to carry it into the ringdown cell. Neopentane is a gas at room temperature and so the desired amount of precursor was adjusted with a regulator. Before entering the cell, O_2 was mixed into the reactant mixture so that as soon as pentyl radicals were produced, the peroxy radical formation step quickly followed. Typical experimental concentrations for this method were $[(COCl)_2] \approx 0.5-1$ Torr, $[C_5H_{12}] = 4$ Torr, $[O_2] = 80$ Torr, and $[N_2] = 150$ Torr. Using the same photolysis flux of 193 nm photons from above (2.2×10^{16} cm^{-2}), the absorption cross section of oxalyl chloride at 193 nm ($\sigma = 3.8 \times 10^{-18}$ cm^2/molecule),[28] and the $[(COCl)_2]$, the number of C_5H_{11} radicals produced from this method is $\approx 5 \times 10^{15}$ cm^{-3}.

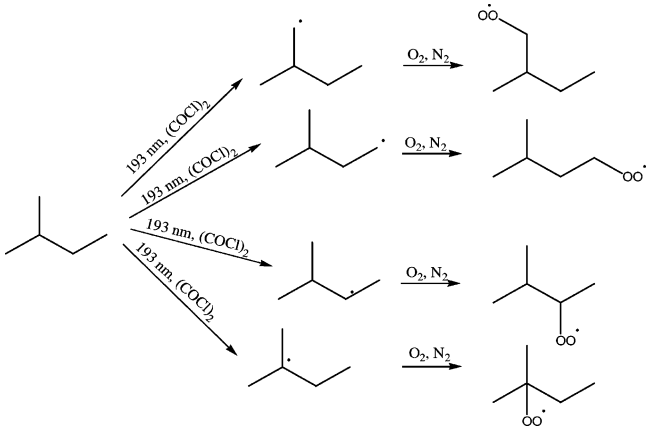

Figure 2. Hydrogen abstraction method illustrated for the four peroxy radicals produced from isopentane. A Cl atom produced from the photolysis of oxalyl chloride abstracts an H atom from four different positions in isopentane to initiate the production of four unique pentyl peroxy radicals.

In comparing the two initiation steps of pentyl peroxy radical production, both methods had advantages and disadvantages. The direct photolysis of $C_5H_{11}Br$, for example, had the advantage of being isomer-specific, which greatly reduced the complexity of the observed spectra, as the observed structure was due to one pentyl peroxy isomer. However, the absorption cross sections of the pentyl bromides are estimated to be approximately 1 order of magnitude smaller than that of oxalyl chloride, which resulted in a better signal-to-noise ratio for the spectra produced from the hydrogen abstraction method. This was further proven in the experiments on neopentyl peroxy, where both production methods were isomer-specific, and the spectra resulting from H-atom abstraction of neopentane by Cl had 2−3 times more signal than those from the direct photolysis of neopentyl bromide, while both had the same noise level. Therefore, utilizing both methods complementarily allowed for not only definitive assignment of the pentyl peroxy isomers' spectra, but also yielded additional information about the reactivity of primary/secondary/tertiary sites in isopentane (see section 5). While not particularly exploited here, the concentration of alkyl bromide precursor is approximately limited by its vapor pressure at room temperature, whereas no such limitation exists in the Cl atom reaction approach.

For these experiments, oxygen (4.3 UHP grade) and nitrogen (5.0 UHP grade) were obtained from Praxair. For the direct photolysis production method, 1-bromopentane (99%), 2-bromopentane (95%), 3-bromopentane (95%), 1-bromo-2-methylbutane (99%), 1-bromo-3-methylbutane (96%), 2-bromo-2-methyl-butane (95%), and 1-bromo-2,2-dimethylpropane (98%) were all purchased from Aldrich and used without further purification. While we cannot be certain that these brominated

samples do not contain impurities that could affect our reaction chemistry and interfere with our spectroscopic results, we think it is unlikely that the pentyl peroxy spectra reported here contain any observed features that are attributable to the precursors' impurities. It is expected that the major impurities in the pentyl bromide compounds are additional isomers (i.e., the 2-bromopentane sample also contains 3-bromopentane), which could introduce some complications into making isomer-specific pentyl peroxy spectral assignments, however, selected pentyl bromide samples were checked by NMR and revealed no observable contribution from other isomers. In addition we have obtained similar spectra for a given pentyl peroxy isomer using two independent production methods. While the pentyl peroxy spectra produced from the H-atom abstraction of isopentane/*n*-pentane contain multiple pentyl peroxy isomers' spectra that overlap, it is still relatively straightforward to confirm some, if not all, of the structures in a particular isomer's spectrum from both production methods.

2-Bromo-3-methylbutane was not available commercially and was, therefore, synthesized by adapting the procedure from Bennett and Bunce[29] (for converting cyclopropylphenylcarbinol to cyclopropylphenylcarbinyl bromide) to convert 3-methyl-2-butanol to 2-bromo-3-methylbutane. The synthesized bromide was purified by distillation and checked by NMR. For the hydrogen abstraction method, oxalyl chloride (98%), *n*-pentane (99%), and isopentane (2-methylbutane, 99%) were also purchased from Aldrich and used without further purification. Neopentane (99%) was purchased from Linde Gas.

3. Spectral Assignments from Previously Studied Alkyl Peroxy Radicals

It is worthwhile briefly reviewing what has been observed and assigned in the NIR CRDS spectra of both ethyl and propyl peroxy radicals, since we will be using the information gained from these as a guide for assigning the spectra of the eight isomers of pentyl peroxy radical.

Previous NIR CRDS studies of the $\tilde{A}-\tilde{X}$ electronic transition for ethyl peroxy radical[21,22] ($C_2H_5O_2$) proved that this technique could distinguish between different conformers of the same peroxy radical. Two bands were observed in the origin region for $C_2H_5O_2$, which were assigned to the electronic origins of the trans (T) and gauche (G) conformers of the radical, of which both are stable minima in the $\tilde{X}$ state potential energy surface (PES) and their separation in energy is small enough that both are populated at room temperature. These conformers have different dihedral angles between the O−O−C and O−C−C planes in the radical: 0° for T and 120° for G. To make the assignments of T and G to the two spectral features observed in the origin region for ethyl peroxy, Miller and co-workers[22] utilized predictions of the $\tilde{A}-\tilde{X}$ transition frequency for each conformer from quantum-chemical calculations (EOMIP-CCSD calculations[30] with a DZP basis set[31]). These assignments were experimentally confirmed by the partially resolved rotational structure in each of the origin bands. In the spectrum of $C_2H_5O_2$, the lower frequency feature was assigned to the electronic origin (0_0^0) of the T conformer and the higher frequency feature to that of the G, with the G origin roughly 3 times more intense than the T. This factor of 3 difference in intensity was attributed partially to the energy separation of the conformers' $\tilde{X}$ states (i.e., the G conformer is predicted to lie 81 cm^{-1} lower in energy than the T). In addition, the G conformer is degenerate, since a dihedral angle of −120° would not be spectroscopically distinct from +120°, thereby adding a factor of 2 to the Boltzmann population of the G conformer origin at 300 K.

In going from ethyl to propyl peroxy radical, adding one CH_2 group results in two peroxy radical isomers, namely 1- and 2-propyl peroxy radicals (1-$C_3H_7O_2$ and 2-$C_3H_7O_2$), with multiple stable conformers expected to be populated at room temperature for each.[23] The five stable conformers of 1-$C_3H_7O_2$, predicted by ab initio calculations, are T_1T_2, T_1G_2, G_1T_2, G_1G_2, and $G_1'G_2$, where $T_1/G_1/G_1'$ indicates the dihedral angle between the O−O−C and O−C−C planes and T_2/G_2 indicates the dihedral angle between the O−C−C and C−C−C planes (0° for T, 120° for G, and −120° for G′). 2-$C_3H_7O_2$ has two stable conformers T and G predicted by calculations as well, where T/G here indicates a 0°/120° dihedral angle between the O−O−C plane and the plane that bisects the C−C−C angle. The resulting NIR spectra for both propyl peroxy isomers, therefore, had multiple peaks present in the origin region. The assignments of these peaks were based upon a combination of the extrapolation of the robust assignment of the 0_0^0 bands for the conformers of $C_2H_5O_2$ and a series of ab initio calculations on $C_3H_7O_2$.

Extensive EOMIP-CCSD calculations were used to predict the energy order of the conformers' $\tilde{A}-\tilde{X}$ transition frequencies, and G2 calculations were used to determine the relative populations of these conformers.[25] Based upon these calculations, the following assignments for 1-$C_3H_7O_2$ were made: peak A (bands labeled alphabetically from lowest to highest frequency) was assigned to the overlap of the T_1T_2 and T_1G_2 conformer origins, peak B to the origin of G_1G_2, and peak C to the overlap of the G_1T_2 and $G_1'G_2$ conformer origins. Like in ethyl peroxy, the lowest frequency band was assigned to T_1 conformers' origins, while the G_1 conformers' lie at higher frequency. In addition, the G_1 peaks were again more intense than the T_1 in 1-$C_3H_7O_2$, likely due to their lower lying $\tilde{X}$ state energy and their degeneracy.

For 2-$C_3H_7O_2$, the lower frequency band was assigned to the G conformer and the higher frequency band to the T, based upon calculations. The G conformer origin was observed to be roughly 10 times more intense than the T, which is partially explained by the $\tilde{X}$ state energy order of the conformers and the presumed degeneracy of the G conformer as well. However, these two together would explain an intensity difference of ≈4, but not a factor of 10. This discrepancy could possibly be due to different Franck−Condon factors for the $\tilde{A}-\tilde{X}$ electronic transition in the G and T conformers of 2-$C_3H_7O_2$ radical.

The higher density of rotational levels of $C_3H_7O_2$ vs $C_2H_5O_2$, plus the overlap of rotational contours of different conformers, precluded the experimental confirmation of the above assignments for 1- and 2-$C_3H_7O_2$ via analysis of their rotational structure.

4. Observed Spectra and Assignments

To sort out the spectra of the pentyl peroxy radicals, the eight isomers have been grouped into primary, secondary and tertiary sets. While both production methods described above were utilized, sections 4.1−4.3 will mainly discuss the observed pentyl peroxy spectra obtained from the isomer-specific production mechanism, where the initiation step was the direct photolysis of alkyl bromides. The spectrum of neopentyl peroxy is the exception to this, since both production methods were isomer-specific and the H-atom abstraction method produced a higher signal-to-noise ratio. For neopentyl peroxy, therefore, the origin spectrum in Figure 3 and the more complete spectrum in Figure 4 are produced by the hydrogen abstraction from neopentane with Cl. Excluding neopentyl peroxy, all other spectra shown in Figures 3, 5, and 6, as well as the frequencies

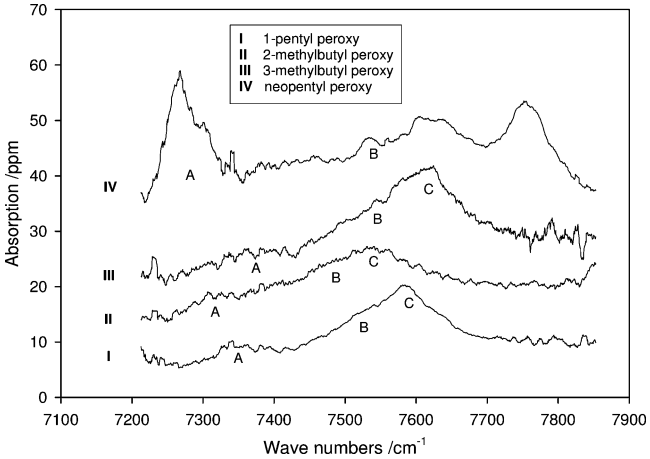

Figure 3. Electronic origin spectra for the four primary pentyl peroxy radicals: 1-pentyl peroxy (I), 2-methylbutyl peroxy (II), 3-methylbutyl peroxy (III), neopentyl peroxy (IV). Traces I, II, and III contain three peaks, labeled A, B, C, which are assigned to unresolved overlaps of different conformers of a given pentyl peroxy isomer. Trace IV contains two origin bands (A, B) that are assigned to two unique conformers of neopentyl peroxy; the assignment of the additional bands are discussed in the text. All spectra have been digitally smoothed to elucidate structure and are manually offset in the y-direction for visualization purposes.

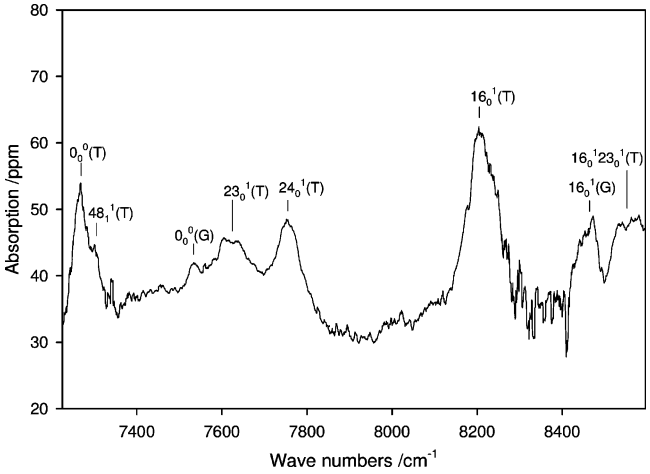

Figure 4. Wide view of the electronic spectrum of neopentyl peroxy. Bands are labeled with the $N^{\upsilon'}_{\upsilon''}$ notation, as defined by Herzberg,[36] where N corresponds to the vibrational mode and υ''/υ' corresponds to the number of quanta in the ground/excited states. 0^0_0(G/T) are the origin bands of the two conformers of neopentyl peroxy. The assigned vibrational bands correspond to the following approximate motions: ν_{48}: OO torsion, ν_{23}: CCC bend + COO bend, ν_{24}: CCC bend + COO bend, and ν_{16}: O−O stretch. The increase in noise from 8300 to 8400 cm^{-1} is due to a strong precursor background absorption.

given in Tables 1, 3, and 4, are obtained using the direct photolysis of pentyl bromides.

4.1. Primary Pentyl Peroxy Radical Isomers. The NIR CRDS spectra of the primary pentyl peroxy radicals (1-pentyl peroxy (I), 2-methylbutyl peroxy (II), 3-methylbutyl peroxy (III), and neopentyl peroxy (IV)) are presented in Figure 3. For traces I, II, and III, there are three peaks resolved, labeled A, B, and C. As was the case for 1-propyl peroxy,[25] 1-butyl peroxy,[24] and isobutyl peroxy,[24] these three peaks are assigned to origins of the $\tilde{A}-\tilde{X}$ electronic transition for different conformers (or sets of conformers) of a given pentyl peroxy isomer. Using the assignments from 1-propyl peroxy,[25] corresponding conformer assignments of the origin peaks in the primary pentyl peroxies' spectra can be made.

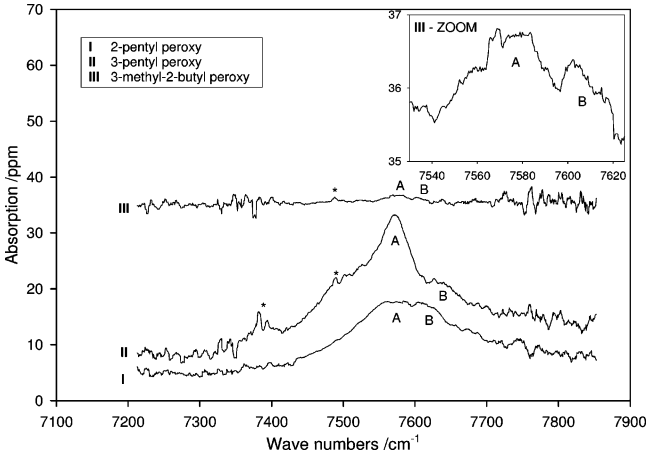

Figure 5. Electronic origin spectra for the three secondary pentyl peroxy radicals: 2-pentyl peroxy (I), 3-pentyl peroxy (II), 3-methyl-2-butyl peroxy (III). Each secondary isomer has two peaks in the origin region (labeled A and B), which are assigned to different conformers of a given pentyl peroxy isomer. The starred features are due to CH_3O_2, which is a byproduct of the production of pentyl peroxy radicals. The region from 7530 to 7625 cm^{-1} in the spectrum of 3-methyl-2-butyl peroxy (III) is zoomed in the inserted box to elucidate conformer origin structure (see section 4.2 for details). All spectra have been digitally smoothed to elucidate structure and are manually offset in the y-direction for visualization purposes.

TABLE 1: Experimental $\tilde{A}-\tilde{X}$ Origin Frequencies[a] (0^0_0) of the Primary Peroxy Isomers from Propyl through Pentyl Peroxy (in cm^{-1})

peroxy isomer	A[b]	B[b]	C[b]	Δ (B−A)	Δ (C−A)
1-propyl[c]	7332	7508	7569	176	237
1-butyl[d]	7355	7525	7591	170	236
isobutyl[d]	7306	7480	7536	174	230
1-pentyl	7351	7523	7586	172	235
2-methylbutyl	7318	7490	7549	172	231
3-methylbutyl	7361	7551	7620	190	259
neopentyl	7267	7534		267	

[a] The uncertainty in these frequencies is estimated to be ±10 cm^{-1}, due to the overlap of multiple conformer origin bands within one observed peak. [b] A, B, and C labels are given to the set of bands that belong to the same pentyl peroxy radical isomer. These bands are assigned to unresolved overlaps of multiple conformer origins (see section 4.1). [c] Reference 25. [d] Reference 24.

Given that the lowest frequency peak was assigned to an unresolved combination of T_1 conformers for 1-$C_3H_7O_2$, we expect that the lowest frequency peak, labeled A, in traces I, II, and III of Figure 3 is likewise due to an unresolved combination of T_1 conformers (0° dihedral angle between O−O−C and O−C−C planes). The spectral width and intensity of peak A is very similar to what was observed for primary propyl peroxy and for both primary butyl peroxy isomers. The number of T_1 conformers for a given primary pentyl peroxy isomer should be greater than the number for primary propyl peroxy, or a primary butyl peroxy isomer, due to more possible orientations of the extended hydrocarbon chain. However, the $\tilde{A}-\tilde{X}$ transitions of the multiple T_1 conformers of the smaller peroxies were not individually resolved, so it is not surprising that the spectral appearance of this A peak is unchanged in going from 1-propyl peroxy to 1-pentyl peroxy. Indeed in comparing the NIR CRDS spectra of 1-propyl and 1-butyl peroxy, there is little change in width or intensity of peak A, even though this peak was tentatively assigned as an overlap of five conformers in 1-butyl peroxy, as opposed to an overlap of two in 1-propyl peroxy.

In increasing frequency, the peaks called B and C were assigned to G_1 conformer origins in 1-$C_3H_7O_2$ (120° dihedral angle between O−O−C and O−C−C planes), with B as the origin of the G_1G_2 conformer and C as an unresolved combination of two other stable G_1 conformers (G_1T_2 and $G_1'G_2$). Therefore, peaks B and C in traces I, II, and III of Figure 3 are assigned to unresolved combinations of the various G_1 conformers, with changes in orientation further down the hydrocarbon chain distinguishing between B and C. Table 1 gives the frequencies of the observed A, B, and C peaks for each primary pentyl peroxy. In addition, columns 5 and 6 give the difference in frequency between peaks B and C, respectively, from peak A. These differences for 1-pentyl peroxy, 2-methylbutyl peroxy, and 3-methylbutyl peroxy are very similar with respect to one another, especially since the error in assigning frequencies to the observed peaks is estimated to be ±10 cm^{-1} (±20 cm^{-1} for 2-methylbutyl peroxy because of its poorer signal-to-noise ratio (S/N)), due to the fact that many conformer origins overlap under a single peak. These frequency separations are also similar to those observed in the spectra of 1-propyl, 1-butyl, and isobutyl peroxies, as seen in Table 1.

The origin spectrum of neopentyl peroxy (trace IV in Figure 3) is clearly different from the other primary pentyl peroxies' spectra. This is largely due to there only being two stable unique conformations of neopentyl peroxy. To describe these conformers, it is easiest to picture neopentyl peroxy as ethyl peroxy, with the 3 H's on the β carbon atom substituted by methyl (CH_3) groups. Therefore, as with $C_2H_5O_2$, neopentyl peroxy should have one unique T and one unique G conformer, and this has been confirmed by ab initio calculations (Gaussian 03W,[32] B3LYP 6-31+G(d)). Unlike $C_2H_5O_2$, calculations predict that the T conformer of neopentyl peroxy lies lower in energy than the G. The two conformers are predicted to be separated by roughly the same energy difference as they were in ethyl peroxy (≈80 cm^{-1}), and hence, we expect that both are populated at room temperature. According to calculations, the optimized G conformer geometry of neopentyl peroxy has an 80° dihedral angle between the O−O−C and O−C−C planes in the $\tilde{X}$ state and a 105° angle in the $\tilde{A}$ state, rather than 120° in both states as in $C_2H_5O_2$. We expect that this significant geometry change between the $\tilde{X}$ and $\tilde{A}$ states gives its $\tilde{A}-\tilde{X}$ transition a poorer Franck−Condon factor than the G conformer of $C_2H_5O_2$ or the T conformer of neopentyl peroxy. Based on our calculations of the neopentyl peroxy conformers' origin frequencies and the ethyl peroxy assignments, we assign peak A in trace IV of Figure 3 to the origin of the T conformer and peak B to that of the G conformer.

The full NIR CRDS spectrum of neopentyl peroxy is given in Figure 4. In addition to the two conformer origin bands, labeled 0_0^0(T) and 0_0^0(G), there is much more structure observed, which can all be assigned to transitions in vibrational modes whose motions contain the peroxy moiety. As was also seen in the smaller alkyl peroxy radicals, because the $\tilde{A}-\tilde{X}$ electronic transition is primarily localized on the outer oxygen (O) atom, we expect to observe fundamental transitions of symmetric vibrations that involve motion of the outer O. In the electronic spectra of the butyl peroxy radicals for example, fundamental transitions in both the COO bend and O−O stretch vibrations were observed at ≈500 and ≈950 cm^{-1}, respectively, blue-shifted from the conformer origin bands.[24] Typically, these vibrational bands are of moderate intensities with respect to the origin, with the O−O stretch band usually more intense than the COO bend.

TABLE 2: Assignments of the $\tilde{A}-\tilde{X}$ Electronic Spectrum of Neopentyl Peroxy[a]

assignment[b]	observed frequency[c]	experimental shift	calculated shift[d]
0_0^0(T)	7267		
48_1^1(T)	7300	+33	+37
0_0^0(G)	7534		
23_0^1(T)	7620	+353	+298
24_0^1(T)	7755	+488	+412
16_0^1(T)	8207	+940	+970
16_0^1(G)	8471	+937	+969
$16_0^1 23_0^1$(T)	8527	+1260	+1268

[a] All frequencies are in units of cm^{-1}. The experimental shifts from the corresponding conformer origin (0_0^0) are compared with those predicted by theory. [b] Bands are labeled with the $N_{\upsilon''}^{\upsilon'}$ notation, as defined by Herzberg,[36] where N corresponds to the vibrational mode number and υ''/υ' corresponds to the number of quanta in the ground/excited states. [c] The uncertainty in these frequencies is estimated to be ±10 cm^{-1}. [d] Shifts derived using the calculated harmonic vibrational frequencies in the ground and/or excited states. These frequencies have been calculated after geometry optimization at the B3LYP/6-31+G(d) level of theory using Gaussian 03W.[32] Gaussian frequencies were scaled by 0.9642, a recommended scaling factor for this level of theory taken from the NIST Computational Comparison: http://srdata.nist.gov/cccbdb/vsf.asp.

Table 2 lists the assignments of all bands observed in Figure 4. With the exception of 48_1^1, the observed vibrational structure is due to fundamental transitions in symmetric vibrational modes whose motions contain the outermost O atom: ν_{16}: O−O stretch, ν_{23}: CCC bend + COO bend, and ν_{24}: CCC bend + COO bend. As seen in Table 2, the experimentally observed transition frequencies are in good agreement with those predicted from ab initio calculations. ν_{48}, whose asymmetric motion is a torsion of the OO group, is the lowest energy vibrational mode in both the $\tilde{X}$ and $\tilde{A}$ states, lying only 50 cm^{-1} higher than the vibrationless level in the ground state, and hence is well populated at room temperature. As seen for the other vibrational band assignments in neopentyl peroxy, there is good agreement between the observed 48_1^1 band and its theoretical prediction (see Table 2). Hot band structure has also been observed previously in the lowest energy modes of both methyl and ethyl peroxies.[21,22]

The assignment of the band at 7620 cm^{-1} to 23_0^1(T) is the most tentative, since there are multiple equally good assignments for this feature, and the band structure is indicative of an overlap of more than one band. In addition to the 23_0^1(T) assignment, 25_0^1(T) is also a good candidate, as ν_{25} is a symmetric mode whose motion includes some COO bending motion in the $\tilde{A}$ state, and its fundamental transition is predicted to be +324 cm^{-1} from the origin. While this prediction is closer to the observed band than 23_0^1(T), the motion of ν_{23} has more COO bending character (as determined by previewing the motions of these vibrational modes with GaussView software[33]) than ν_{25}. While the assignment of 23_0^1(T) was chosen here, we recognize the possibilities of 25_0^1(T) as an alternate assignment for this band and that both 23_0^1(T) and 25_0^1(T) could be present and overlapping in the band observed at 7620 cm^{-1}. Additionally, the doublet structure of this band is similar to that observed in the origin band of the T conformer, and hence could also be assigned to both 23_0^1(T) and 23_0^1(T) in combination with 48_1^1(T). Given this band's moderately weak intensity and the lack of baseline resolution between the doublet, it is difficult to make more than one assignment to this feature. The relatively good agreement between the experimental shift and the calcu-

lated shift for the combination band $16_0^1 23_0^1$(T) in Table 2 also lends some support to the 23_0^1(T) assignment for the band at 7620 cm^{-1}.

With the exception of 0_0^0(G) and 16_0^1(G), all assigned bands are due to the T conformer. It is not surprising that we do not observe the corresponding transitions for the G conformer, since the G origin is much weaker than the T, and these vibrational bands would likely be weaker than the origin.

4.2. Secondary Pentyl Peroxy Radical Isomers. The NIR CRDS spectra of the secondary pentyl peroxy radicals (2-pentyl peroxy, 3-pentyl peroxy, and 3-methyl-2-butyl peroxy) are presented in Figure 5. For all three isomers, two peaks are resolved, which partially overlap, and are labeled A and B. As was the case for 2-propyl[25] and 2-butyl[24] peroxy, these two peaks are assigned to origins of the $\tilde{A}-\tilde{X}$ electronic transition for different conformers of a given pentyl peroxy isomer. Using the assignments of 2-propyl peroxy,[25] which were based on extensive quantum-chemical calculations, corresponding conformer assignments of the two origin peaks in the secondary pentyl peroxies' spectra can be made.

Before assigning the spectra, there are two features present in Figure 5, which require more explanation. The S/N in the spectrum of 3-methyl-2-butyl peroxy (III) is much worse than that of 2-pentyl peroxy (I) and 3-pentyl peroxy (II) because of the smaller signal intensities of the A and B peaks in 3-methyl-2-butyl peroxy. The lower peak intensities in trace III compared to I and II are attributed to poorer sample purity of the precursor, since unlike 2- and 3-bromopentane, which were purchased in high purity from Aldrich, 2-bromo-3-methylbutane had to be synthesized. Therefore, a zoom of the A and B peaks in trace III is contained in the inserted box. In the spectra of 3-pentyl peroxy and 3-methyl-2-butyl peroxy, the starred features belong to methyl peroxy (CH_3O_2), which is a byproduct of the production of pentyl peroxy radicals. This CH_3O_2 byproduct was also observed in previous NIR CRDS studies of ethyl,[22] propyl,[23] and butyl[24] peroxy radicals.

In 2-$C_3H_7O_2$, the lower frequency peak was assigned to the G conformer origin, corresponding to the conformation where the C−O−O plane and the plane that bisects the C−C−C angle lie at 120° from each other. The corresponding lower frequency peak, labeled A in the secondary pentyl peroxies' spectra, is therefore also assigned to the G conformer(s) origin(s). While 2-propyl peroxy possesses only one G conformer, it is expected that multiple G conformers (corresponding to different orientations of the hydrocarbon "tail") of each secondary pentyl peroxy isomer should be stable and populated at room temperature. Therefore, the A peaks in all three spectra in Figure 5 are assigned to an unresolved overlap of G conformer origins for a given pentyl peroxy isomer. A similar situation was observed in the origin spectrum of 2-$C_4H_9O_2$, where multiple G conformer origins were assigned to a single peak.[24]

The higher frequency peak in 2-$C_3H_7O_2$ was assigned to the T conformer origin, corresponding to the conformation where the dihedral angle between the C−O−O plane and the plane that bisects the C−C−C angle is 0°. Accordingly, peak B in the secondary pentyl peroxies' spectra is also assigned to T conformer origin(s). As was already observed in going from 2-propyl to 2-butyl peroxy, lengthening the hydrocarbon chain increases the number of stable T conformers possibly populated at room temperature. Further lengthening the hydrocarbon chain from 2-butyl to 2-pentyl peroxy is expected to have a similar effect. Therefore, peak B is assigned to an unresolved overlap of T conformer origins.

TABLE 3: Experimental $\tilde{A}-\tilde{X}$ Origin Frequencies[a] (0_0^0) of the Secondary Peroxy Isomers from Propyl through Pentyl Peroxy (in cm^{-1})

peroxy isomer	A[b]	B[b]	Δ (B−A)
2-propyl	7567[c]	7701[d]	134
2-butyl[e]	7560	7605	45
2-pentyl	7564	7613	49
3-pentyl	7572	7643	71
3-methyl-2-butyl	7577	7606	29

[a] The uncertainty in these frequencies is estimated to be ±10 cm^{-1}, due to the overlap of multiple conformer origin bands within one observed peak. [b] A and B labels are given to two bands that belong to the same pentyl peroxy radical isomer. These bands are assigned to unresolved overlaps of multiple conformer origins (see section 4.2). [c] Reference 25. [d] Remeasured, ref 25 gives 7692 cm^{-1} [e] Reference 24.

The intensity ratio of the G and T origin peaks in 2-propyl peroxy is quite different from that observed in the secondary pentyl peroxies' spectra. In 2-$C_3H_7O_2$, the G conformer origin was roughly 10 times more intense than the T (see section 3), while only an intensity difference of 4:1 was expected, based on the calculated energies of the conformers and their Boltzmann populations at 300 K. While the A:B (or G:T) ratio varies slightly among the three secondary pentyl peroxies' origin spectra, in all cases it is much closer to unity. Since we have no calculations for the conformer energies in the larger peroxy radicals, it is impossible to say how well this observation agrees with expectations.

Table 3 gives the frequencies of the observed A and B peaks for each secondary pentyl peroxy. In addition, column 4 gives the difference in frequency between these two peaks. These Δ-(B-A) values for all three secondary pentyl peroxy isomers are very similar with respect to one another, especially since the error in assigning frequencies to the observed peaks is estimated to be ±10 cm^{-1}, due to the fact that many conformer origins overlap under a single peak. These frequency separations (in the range of 30−70 cm^{-1}) are also in relatively good agreement with that observed for 2-propyl and 2-butyl peroxies, as seen in Table 3. In addition to their similar A:B intensity ratios mentioned above, the agreement in the separation between these conformer peaks in the secondary pentyl peroxies' spectra lends additional evidence that these assignments are valid.

4.3. Tertiary Butyl and Pentyl Peroxy Radicals. Unlike for the primary and secondary pentyl peroxies, there have not been corresponding conformeric assignments made for another tertiary alkyl peroxy's origin spectrum, which were based on extensive quantum-chemical calculations. Indeed in the previous study of *t*-butyl peroxy, the smallest tertiary alkyl peroxy radical, the observed spectrum was not completely understood.[24] To estimate the number of possible stable conformers for *t*-butyl peroxy without doing calculations, Glover and Miller[24] utilized the fact that *t*-butyl peroxy is structurally similar to methyl peroxy, with each H connected to C−O−O substituted by CH_3 groups. Therefore, this yields only two possible unique conformations: one where the oxygens in the peroxy group are staggered with respect to the CH_3 groups and one where they are eclipsed. While in CH_3O_2 the eclipsed conformer is a saddle point in the PES,[34] and therefore only the staggered conformer contributes to the electronic spectrum, it was not clear that this would necessarily also be true for *t*-butyl peroxy. In fact, Glover and Miller observed a total of four peaks in the origin region of the *t*-butyl peroxy electronic spectrum,[24] but the assignment of all four peaks to particular conformers was not reported, since only two conformers were expected. Before attempting to analyze the spectrum of *t*-pentyl peroxy, it seems logical to first

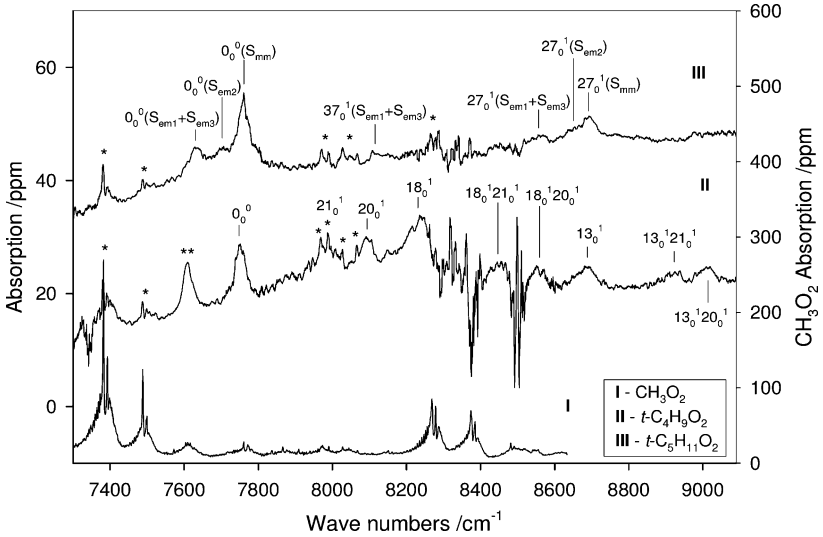

Figure 6. Full electronic spectra for (I) methyl peroxy (CH_3O_2), (II) *t*-butyl peroxy (*t*-$C_4H_9O_2$), and (III) *t*-pentyl peroxy (*t*-$C_5H_{11}O_2$). The single-starred features in II and III are due to methyl peroxy (I), which is a byproduct of the production of butyl/pentyl peroxy radicals. The double-starred peak in II was previously assigned to an unknown byproduct,[24] which was also observed in the electronic spectrum of isobutyl peroxy. Assigned bands in II and III are labeled with the $N_{\upsilon''}^{\upsilon'}$ notation, as defined by Herzberg,[36] where *N* corresponds to the vibrational mode and υ''/υ' corresponds to the number of quanta in the ground/excited states. The *t*-$C_4H_9O_2$ spectrum contains a single conformer origin (0_0^0) and several fundamental transitions and combinations bands in the following vibrational modes: ν_{21}: CCO bend + COO bend, ν_{20}: CCC bend + COO bend, ν_{18}: COO bend, and ν_{13}: asymmetric C−O−O stretch. The *t*-$C_5H_{11}O_2$ spectrum contains three resolved origin bands (labeled 0_0^0(S...)) for its four stable conformers: S_{mm}, S_{em1}, S_{em2}, S_{em3} (see Figure 7). In addition, conformer-specific COO bend (37_0^1) and O−O stretch vibrational bands (27_0^1) are also observed. The increase in noise from 8200 to 8500 cm^{-1} in II and III is due to strong precursor absorptions. All three spectra have been digitally smoothed to elucidate structure and are manually offset in the *y* direction for visualization purposes.

complete the analysis on the spectrum of the smallest tertiary peroxy radical: *t*-butyl peroxy.

Ab initio calculations were performed to identify the actual number of stable, unique conformers of *t*-butyl peroxy (*t*-$C_4H_9O_2$). Using the B3LYP method (6-31+G(d) basis set) of Gaussian 03W,[32] we ran a PES calculation where the CCOO dihedral angle was scanned from a staggered geometry of the molecule, through an eclipsed orientation, to again a staggered position, and the geometry was optimized at each CCOO angle in the scan. This resulted in a single global minimum geometry, where the CCOO dihedral angle is 60° or 180°, corresponding to a staggered position of the OO between two CH_3 groups. Like in CH_3O_2, the eclipsed orientation of *t*-$C_4H_9O_2$ is a saddle point on the PES. At this same level of theory, frequency calculations were also performed for both the $\tilde{X}$ and $\tilde{A}$ electronic states of the staggered conformer.

The full NIR CRDS spectrum of *t*-$C_4H_9O_2$ is trace II in Figure 6. The region of the spectrum from 7300 to 8700 cm^{-1} agrees well with that reported previously.[24] The single-starred features in the spectrum are all due to CH_3O_2, as seen by comparing trace II with the spectrum of CH_3O_2 (trace I). The intensities of this CH_3O_2 structure are indicative of it being produced vibrationally hot, since the intensity ratio of the origin band at 7383 cm^{-1} and the vibrational bands at ≈8000 cm^{-1} is greatly different between traces I and II. We know that CH_3O_2 is a byproduct of the production of butyl peroxy radicals, but we are currently investigating its exact production mechanism in these larger alkyl peroxy experiments because of this intensity ratio difference between the CH_3O_2 structure in traces I and II and that trace I is CH_3O_2 at 300 K. The double-starred feature in trace II was also observed in the electronic spectrum of isobutyl peroxy and was previously assigned as a stable byproduct,[24] due to its different kinetic behavior from the butyl peroxy signals.

In addition to the band identified in Figure 6 as the origin (0_0^0) of the $\tilde{A}-\tilde{X}$ electronic transition, there are many vibrational bands observed in the spectrum of *t*-$C_4H_9O_2$. As seen in neopentyl peroxy and in the smaller peroxy radicals, the additional structure can be assigned to fundamental vibrational transitions in modes whose motion involves displacement of the outer O atom: ν_{21}: CCO bend + COO bend, ν_{20}: CCC bend + COO bend, ν_{18}: COO bend, and ν_{13}: O−O stretch. The COO bend and O−O stretch vibrations were also observed for the other isomers of butyl peroxy at ≈500 and ≈950 cm^{-1} to the blue of their respective origin bands.[24] Table 4 lists all of the vibrational bands observed in the spectrum of *t*-$C_4H_9O_2$ with their experimental shifts from 0_0^0 compared to ab initio predictions, and these are in good agreement in all cases. 18_0^1 and 13_0^1 correspond to fundamental transitions in the COO bend and O−O stretch vibrations, and their experimental shifts from 0_0^0 are also in good agreement with those observed for the other butyl peroxy isomers previously. 21_0^1 and 20_0^1 both overlap the dense CH_3O_2 structure at ≈8000 cm^{-1}, which could account for some of the increased intensity of these CH_3O_2 vibrational bands with respect to the origin. However, even with the overlap of broad *t*-$C_4H_9O_2$ structure, the intensity ratio between these methyl peroxy vibrational bands and its origin is still nonequilibrium at room temperature.

The full NIR CRDS spectrum of *t*-$C_5H_{11}O_2$ is trace III in Figure 6. While the expectation was that traces II and III would be very similar since they are both spectra of tertiary peroxies, their comparison shows that there are differences. However, one similarity is the presence of CH_3O_2 structure both in the origin (7383 cm^{-1}) and in the ≈8000 cm^{-1} regions. Like in trace II, the intensity ratios of these features suggests that CH_3O_2 is observed vibrationally hot. Also, there is a strong background precursor absorption from ≈8200−8500 cm^{-1} in both traces II and III, which causes an increase in the noise in that region of the spectra. Unlike trace II, trace III has three overlapping peaks of differing intensity in the origin region, and all three lie in close proximity to 0_0^0 of *t*-$C_4H_9O_2$. In attempting to estimate

TABLE 4: Assignments of the $\tilde{A}-\tilde{X}$ Electronic Spectra of *t*-Butyl and *t*-Pentyl Peroxies[a]

peroxy	assignment[b]	observed[c]	experimental shift	calculated shift[d]
t-butyl	0_0^0	7755		
	21_0^1	7995	+240	+232
	20_0^1	8095	+340	+333
	18_0^1	8236	+481	+474
	$18_0^1 21_0^1$	8444	+689	+706
	$18_0^1 20_0^1$	8556	+801	+807
	13_0^1	8689	+934	+958
	$13_0^1 21_0^1$	8924	+1169	+1190
	$13_0^1 20_0^1$	9011	+1256	+1291
t-pentyl	$0_0^0(S_{em1} + S_{em3})$	7632		
	$0_0^0(S_{em2})$	7705		
	$0_0^0(S_{mm})$	7761		
	$37_0^1(S_{em1} + S_{em3})$	8109	+477	+471(S_{em1})/ +433(S_{em3})
	$27_0^1(S_{em1} + S_{em3})$	8565	+933	+959(S_{em1})/ +965(S_{em3})
	$27_0^1(S_{em2})$	8644	+939	+956
	$27_0^1(S_{mm})$	8692	+931	+961

[a] All frequencies are in units of cm^{-1}. The experimental shifts from the corresponding conformer origins (0_0^0) are compared with those predicted by theory. [b] Bands are labeled with the $N_{\upsilon''}^{\upsilon'}$ notation, as defined by Herzberg,[36] where N corresponds to the vibrational mode number and υ''/υ' corresponds to the number of quanta in the ground/excited states. [c] The uncertainty in these frequencies is estimated to be ± 10 cm^{-1}. [d] Shifts derived using the calculated harmonic vibrational frequencies in the ground and/or excited states. These frequencies have been calculated after geometry optimization at the B3LYP/6-31+G(d) level of theory using Gaussian 03W.[32] Gaussian frequencies were scaled by 0.9642, a recommended scaling factor for this level of theory taken from the NIST Computational Comparison: http://srdata.nist.gov/cccbdb/vsf.asp.

the possible conformers for *t*-$C_5H_{11}O_2$, it is not that surprising that there are multiple conformer origins observed in its $\tilde{A}-\tilde{X}$ electronic spectrum, since unlike *t*-$C_4H_9O_2$ where the H's on the C−O−O group of CH_3O_2 have all been replaced by CH_3 groups, *t*-$C_5H_{11}O_2$ breaks that symmetry by substituting two CH_3 groups and one ethyl (C_2H_5) group. Therefore, even if only staggered conformations of *t*-pentyl peroxy correspond to stable minima, as was the case for both methyl and *t*-butyl peroxies, there are likely multiple unique staggered minima because of this asymmetry.

Like for *t*-$C_4H_9O_2$, ab initio calculations were performed to identify the stable, unique conformers of *t*-$C_5H_{11}O_2$. Using the B3LYP method (6-31+G(d) basis set) of Gaussian 03W,[32] we ran a PES calculation where the CCOO dihedral angle was scanned from a staggered geometry of the molecule (i.e., the OO was staggered between two CH_3 groups) to an eclipsed geometry (i.e., the OO was eclipsed with C_2H_5). This PES scan passed through a second staggered geometry, where the OO was staggered between CH_3 and C_2H_5, and a second eclipsed geometry, where OO was eclipsed with CH_3, on route to its stopping point. Additionally, because this C_2H_5 group adds another degree of freedom to the geometry of *t*-$C_5H_{11}O_2$, at each CCOO dihedral angle step in the PES scan, the ethyl group was rotated 360° to find all possible minima. As before, the geometry was optimized at each point in this 2D PES scan.

Figure 7 shows the four unique minima of *t*-$C_5H_{11}O_2$ found from the PES calculation. All four have staggered geometries: one has the OO staggered between two CH_3 groups (S_{mm}) and three of the four have the OO staggered between C_2H_5 and CH_3 (S_{em1}, S_{em2}, and S_{em3}). (Actually there are in principle two

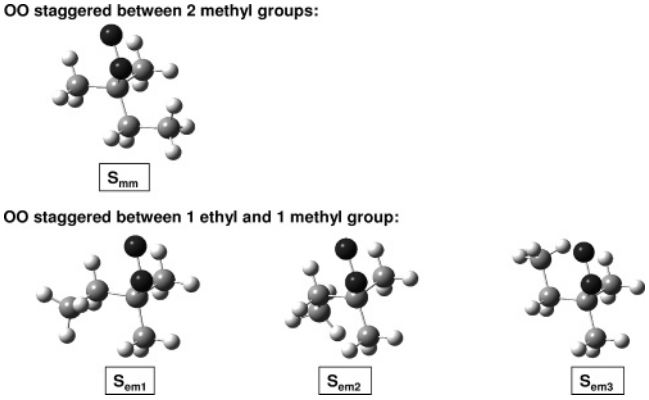

Figure 7. Four stable staggered conformers of *t*-pentyl peroxy predicted by ab initio calculations. Here S refers to a staggered conformation of the OO group and the subscripts mm or em indicate that the oxygens are staggered between two methyl groups (mm) or between an ethyl and a methyl group (em).

spectroscopically distinct S_{mm} conformations but, as discussed below, we expect their transition frequencies likely to be unresolvable.) Like in CH_3O_2 and *t*-$C_4H_9O_2$, the eclipsed orientations are saddle points on the PES. The energy order of these conformers predicted by theory is: $S_{em1} < S_{mm} < S_{em2} < S_{em3}$. The three lowest energy conformers are within <100 cm^{-1} of each other, while S_{em3} is ≈ 400 cm^{-1} higher in energy than S_{em1}. Despite this energy difference being larger than kT at 300 K, we are not at all certain that we achieve equilibrium population of the conformers at this temperature, and hence it is likely that the structure observed in its $\tilde{A}-\tilde{X}$ electronic spectrum might be due to all four stable conformations of *t*-$C_5H_{11}O_2$. At this same level of theory, geometry optimizations, energy calculations, and vibrational frequency calculations were also performed for the $\tilde{X}$ and $\tilde{A}$ electronic states of all four conformers. While we have seen in the studies on smaller alkyl peroxies[35] that the G2 computational method is usually the most accurate in predicting the $\tilde{A} - \tilde{X}$ transition frequency, this method can only be used straightforwardly to calculate the $\tilde{A}$ electronic states for peroxies with C_s symmetry. Therefore, since all four conformers of *t*-$C_5H_{11}O_2$ have C_1 symmetry, we have used the B3LYP method to make transition frequency predictions. While B3LYP gives less accurate absolute transition frequency predictions than G2, it still may give a reliable order of these conformers' transition frequencies.

The calculated $\tilde{A}-\tilde{X}$ frequencies of the *t*-$C_5H_{11}O_2$ conformers are as follows: $S_{mm} = 7865$ cm^{-1}, $S_{em1} = 7792$ cm^{-1}, $S_{em2} = 7924$ cm^{-1}, and $S_{em3} = 7744$ cm^{-1}. Therefore, the three overlapping peaks around ≈ 7700 cm^{-1} in trace III of Figure 6 are assigned to the origin bands of all four conformers of *t*-$C_5H_{11}O_2$, since they are all predicted within a couple hundred wave numbers of each other. The lowest frequency band at 7632 cm^{-1} is assigned to an overlap of 0_0^0 for S_{em1} and 0_0^0 for S_{em3} since these two conformers are predicted to have the lowest $\tilde{A} - \tilde{X}$ transition frequencies, which are within ≈ 50 cm^{-1} of each other.

This assignment leaves two conformers, S_{em2} and S_{mm}, to assign to the remaining two bands. The assignment of the strongest origin band at 7761 cm^{-1} to S_{mm} is supported by several arguments. This band's position agrees relatively well with its predicted transition frequency and with the origin frequency of *t*-$C_4H_9O_2$ (7755 cm^{-1}). S_{mm} is the *t*-$C_5H_{11}O_2$ conformer that is most geometrically similar to the stable staggered conformation of *t*-$C_4H_9O_2$, and hence their similar $\tilde{A}-\tilde{X}$ transition frequencies are consistent with the expectation

that the substitution of a CH_3 group on an H atom far from the peroxy moiety should have little effect on the origin frequency. The greater intensity for $0_0^0(S_{mm})$ compared to the other origin bands is consistent with it being one of the three low-energy conformers and its degeneracy factor, i.e., there are two possible S_{mm} conformers with a CCCO dihedral angle of $\pm 60°$, which would be indistinguishable from each other. A third S_{mm} conformer with a CCCO dihedral angle of 180° is also stable, and while being geometrically unique from the other S_{mm} conformation, our PES calculation indicates that their $\tilde{X}$ state energies are all degenerate within the resolution of our B3LYP computational method. We do not assign this second possible S_{mm} conformer to a unique origin band in our spectrum, but rather we think it contributes to the greater intensity of $0_0^0(S_{mm})$. However, we recognize that degenerate $\tilde{X}$ state energies do not necessarily mean degenerate $\tilde{A}-\tilde{X}$ transition frequencies. Attempts were made to calculate the $\tilde{A}$ state for this conformer to determine its transition frequency but all were unsuccessful because they converged to the $\tilde{X}$ rather than the $\tilde{A}$ state. This leaves the origin band of S_{em2}, which is assigned to the middle peak at 7705 cm^{-1}. It is predicted to have the highest transition frequency, but based on the intensity of these bands and on the fact that the B3LYP predicted transition frequency order, involving small differences of large numbers, may not be taken as completely reliable, we prefer the assignment of the middle origin band to S_{em2} and the bluest origin band rather to S_{mm}.

In addition to the conformer origin bands, there are also O−O stretch vibrational bands assigned for all four conformers (labeled 27_0^1 in trace III). Again, the first of three resolved O−O stretch peaks is assigned to an overlap of 27_0^1 for S_{em1} and S_{em3}, similar to the origin region. There is also one COO bend vibrational mode assigned as 37_0^1 ($S_{em1} + S_{em3}$). While we would expect to see COO bend transitions for all four conformers, there is prominent CH_3O_2 O−O stretch structure at ≈8250 cm^{-1} which likely limited our ability to observe the remaining two COO bend vibrational bands. Given the weak intensity of $37_0^1(S_{em1} + S_{em3})$, it is not surprising that this CH_3O_2 vibrational structure somewhat buries the remaining two COO bend bands. Likewise, there is a strong precursor absorption between 8200 and 8400 cm^{-1}, which also interferes with observing additional vibrational structure. Table 4 lists all the vibrational bands observed in trace III of Figure 6 with their experimental shifts from the corresponding 0_0^0 compared to ab initio predictions, and these are in good agreement in all cases.

5. Reactivity Studies

Given that we are able to make specific spectral assignments to isomers and conformers in the $\tilde{A}-\tilde{X}$ spectra of the pentyl peroxy radicals, we also have the ability to use our spectroscopic studies to gain some kinetic information about these radicals. We recognize that our CRDS apparatus is optimized for spectroscopic and not kinetic studies, thereby limiting the quantitative kinetic information we can obtain from our data. Nevertheless, as was seen in the butyl peroxy experiments,[24] the CRDS studies of the pentyl peroxy radicals can potentially yield semiquantitative kinetic information on their formation chemistry.

In the butyl peroxy studies, a reactivity ratio was reported for the H atoms in butane and isobutane based on the comparison of CRDS spectra obtained for the individual butyl peroxy isomers (using the direct photolysis production method) with the spectra resulting from the Cl atom reaction on butane

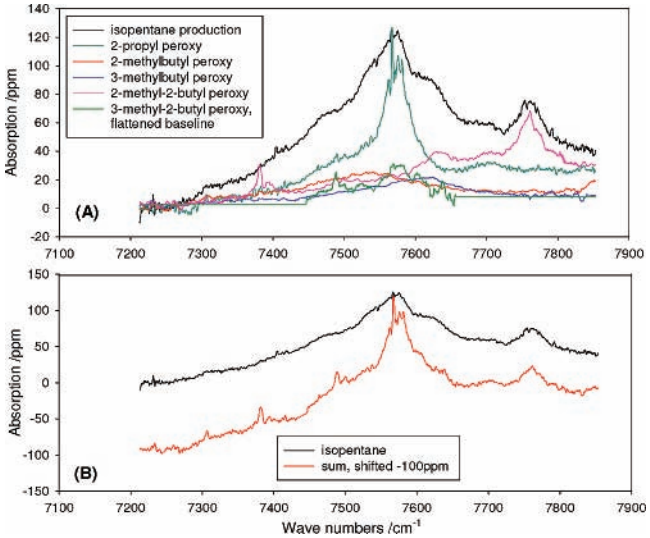

Figure 8. Spectra used for reactivity ratio studies in isopentane (see section 5). Panel A shows a comparison between the CRDS spectrum obtained from the H-atom abstraction of isopentane (black trace) and the scaled individual isopentyl peroxy isomers' spectra obtained from the direct photolysis of their corresponding pentyl bromides. The CRDS spectra for 2-methylbutyl peroxy (red trace), 3-methylbutyl peroxy (dark blue trace), 3-methyl-2-butyl peroxy (green trace), and 2-methyl-2-butyl (*t*-pentyl) peroxy (pink trace) have been scaled by a factor determined from the number and reactivity ratio of primary, secondary, and tertiary H atoms in isopentane. The light blue trace, also in panel A, is the electronic origin spectrum for 2-propyl peroxy, a byproduct from the production of isopentyl peroxy radicals. Panel B compares the sum of the weighted isomers' spectra and the 2-propyl peroxy spectrum (red trace) with that from the H-atom abstraction of isopentane (black trace). The red trace has been manually offset in panel B for visualization purposes. All spectra have been digitally smoothed to elucidate structure.

or isobutane. For example, by applying a weighting factor of 3:1 to the isomer-specific CRDS spectra of 2-butyl (*sec*-butyl) and 1-butyl (*n*-butyl) peroxy, respectively, Glover and Miller[24] were able to qualitatively reproduce the spectrum obtained from the H-atom abstraction of butane by Cl, where both isomers are produced simultaneously. In doing the same for isobutane and its respective butyl peroxy isomers (1:1 weighting factor applied there for isobutyl:*t*-butyl), and then taking into account the number of H's of each type (primary (p), secondary (s), tertiary (t)) in the butane/isobutane molecule, the relative reactivity for Cl atom abstraction of H atoms in butane/isobutane was determined to be 2:9:18 p:s:t, under the assumption that the hydrocarbon radical is quantitatively converted to the corresponding peroxy isomer.

To cross-check this reported reactivity ratio with our pentyl peroxy experiments, we compared the CRDS spectrum obtained from the H-atom abstraction of isopentane with the isomer-specific spectra for the four pentyl peroxy isomers possible from isopentane, namely 2-methylbutyl, 3-methylbutyl, 3-methyl-2-butyl, and 2-methyl-2-butyl (*t*-pentyl) peroxies. Panel A of Figure 8 shows the CRDS spectrum from the Cl atom attack on isopentane in black with the scaled (see below) individual isomers' spectra from the direct photolysis production method in red, dark blue, green and pink. It is clear after comparing the black trace with the individual isomers' that the largest feature at 7567 cm^{-1} is not explainable using only the spectral features of the pentyl peroxies. Both the frequency position and band contour of this peak led us to assign the additional structure to the electronic origin of the G conformer of 2-propyl peroxy, reported earlier.[25] The electronic spectrum for 2-$C_3H_7O_2$ from

the direct photolysis of 2-C_3H_7Br is also shown in panel A of Figure 8 in light blue. To determine the source of 2-$C_3H_7O_2$, the $(COCl)_2$ was removed from the usual $C_5H_{12}/(COCl)_2/O_2/N_2$ experimental conditions, and the resulting CRDS spectrum had no observable pentyl peroxy features, as expected, as well as no 2-propyl peroxy signal. Therefore, one has to conclude that 2-$C_3H_7O_2$ must be formed from the production of isopentyl and/or isopentyl peroxy radicals. Interestingly enough, however, there are no 2-$C_3H_7O_2$ spectral features observed in any of the corresponding isomer-specific spectra.

To determine what weighting factors should be applied to the individual spectra in order to have them accurately sum up the black trace in panel A, we first counted the number of H atoms in isopentane of each type: p, s, and t. This gives a ratio of 9:2:1 (p:s:t); however, there are two different "types" of primary H's, with abstraction of each leading to different primary pentyl peroxy isomers. Therefore, we divide these 9 primary H's into a set of 6, which can make 2-methylbutyl peroxy, and a set of 3, which can make 3-methylbutyl peroxy, yielding a modified count of p:s:t H's in isopentane of 6 + 3:2:1. Multiplying this ratio of H's by the reported butyl peroxy reactivity ratio (2:9:18, p:s:t) determines the following weighting factors for the isopentyl peroxy isomers' spectra: 12:6:18:18 or 2:1:3:3 for 2-methylbutyl peroxy:3-methylbutyl peroxy:3-methyl-2-butyl peroxy:*t*-pentyl peroxy. Panel A of Figure 8 shows the individual isomers' spectra scaled by the appropriate weighting factors. For 3-methyl-2-butyl peroxy (green trace), an additional factor of 5 was applied to bring this spectrum to the same initial intensity scale as the other three isopentyl peroxy isomers before applying the kinetic factor determined above. This extra factor of 5 then increases the noise in the green trace as well, so the baseline has been flattened out to avoid adding in this artificially amplified noise when summing up the individual isomers' traces. Panel B shows the sum of the weighted isomers' spectra plus the spectrum of 2-propyl peroxy, in red, compared with the CRDS spectrum from H-atom abstraction of isopentane, in black. It is clear that the weighted sum of the individual isomers' traces plus the 2-$C_3H_7O_2$ trace reproduces, semiquantitatively, the spectrum from isopentane. Therefore, this estimated reactivity ratio reported in the butyl peroxy studies is confirmed by the pentyl peroxy results.

We had hoped to do more reactivity ratio studies using the H-atom abstraction of *n*-pentane, and comparing that with the individual isomers' spectra for 1-pentyl, 2-pentyl, and 3-pentyl peroxies. However, the spectrum from the Cl atom attack on *n*-pentane yielded only one unresolved spectral feature in the origin region, making it impossible to identify the spectral contribution of the individual isomers.

6. Conclusion

In conclusion, the $\tilde{A}-\tilde{X}$ electronic spectra for the eight isomers of pentyl peroxy radical are reported for the first time using CRDS. Origin transitions for various conformers of each isomer have been assigned principally by extending the assignments of previously studied smaller alkyl peroxies. In addition, conformer-specific vibrational bands have been assigned for neopentyl, *t*-butyl, and *t*-pentyl peroxies, where the observed transitions are due to vibrational modes whose motions involve the outer oxygen atom in the peroxy radical. Two methods of pentyl radical production were used to initiate the formation chemistry of pentyl peroxy radical. The first method involved the direct photolysis of a specific isomer of pentyl bromide to produce the corresponding pentyl radical, which was converted to the peroxy radical. The second method involved the abstraction of a hydrogen atom from pentane to produce a mixture of pentyl radical isomers. Using the two production methods complementarily, we were able to not only make spectral assignments to a particular isomer and conformer of pentyl peroxy radical, but we were also able to confirm the relative reactivities of primary, secondary, and tertiary H's in isopentane.

Acknowledgment. We acknowledge the financial support of this work by the DOE via Grant DE-FG02-01ER14172. E.S. gratefully acknowledges Erica L. Campbell from Dr. Robert Coleman's research group at The Ohio State University, who assisted her with the synthesis of 2-bromo-3-methylbutane and with taking NMR spectra. The authors would also like to acknowledge Gabriel M. P. Just for doing initial ab initio calculations on the G and T conformer $\tilde{X}$ states for 1-butyl, 1-pentyl, and neopentyl peroxies.

References and Notes

(1) Wang, S.; Miller, D. L.; Cernansky, N. P.; Curran, H. J.; Pitz, W. J.; Westbrook, C. K. *Combust. Flame* **1999**, *118*, 415.

(2) Curran, H. J.; Gaffuri, P.; Pitz, W. J.; Westbrook, C. K. *Combust. Flame* **1998**, *114*, 149.

(3) Lightfoot, P. D.; Cox, R. A.; Crowley, J. N.; Destriau, M.; Hayman, G. D.; Jenkin, M. E.; Moortgat, G. K.; Zabel, F. *Atmos. Environ.* **1992**, *26A*, 1805.

(4) Wallington, T. J.; Dagaut, P.; Kurylo, M. J. *Chem. Rev.* **1992**, *92*, 667.

(5) Frost, G. J.; Ellison, G. B.; Vaida, V. *J. Phys. Chem. A* **1999**, *103*, 10169.

(6) Pilling, M. J.; Smith, I. W. M. In *Modern Gas Kinetics: Theory, Experiment, and Application*; Blackwell Scientific Publications: Oxford, New York, 1987; Chapters C1 and C2.

(7) Robertson, S. H.; Seakins, P. W.; Pilling, M. J. In *Low-temperature combustion and autoignition*; Elsevier: Amsterdam, 1997; Chapter 2.

(8) D'Anna, A.; Violi, A.; D'Alessio, A. *Combust. Flame* **2000**, *121*, 418.

(9) Kee, R. J.; Coltrin, M. E.; Glarborg, P. In *Chemically Reacting Flow: Theory and Practice*; John Wiley and Sons: New Jersey, 2003; Chapter 14.

(10) Gaffuri, P.; Faravelli, T.; Ranzi, E.; Cernansky, N. P.; Miller, D.; D'Anna, A.; Ciajolo, A. *Am. Inst. Chem. Eng.* **1997**, *43*, 1278.

(11) Sun, H.; Bozzelli, J. W. *J. Phys. Chem. A* **2004**, *108*, 1694.

(12) DeSain, J. D.; Klippenstein, S. J.; Taatjes, C. A. *Phys. Chem. Chem. Phys.* **2003**, *5*, 1584.

(13) Wallington, T. J.; Andino, J. M.; Potts, A. R.; Nielsen, O. J. *Int. J. Chem. Kinet.* **1992**, *24*, 649.

(14) Wallington, T. J.; Nielsen, O. J. In *Peroxyl Radicals*; John Wiley and Sons: New York, 1997; Chapter 15.

(15) Burggraf, L. W.; Firestone, R. F. *J. Phys. Chem.* **1974**, *78*, 508.

(16) Nielsen, O. J.; Ellermann, T.; Wallington, T. J. *Chem. Phys. Lett.* **1993**, *203*, 302.

(17) Dagaut, P.; Kurylo, M. J. *Int. J. Chem. Kinet.* **1990**, *22*, 1177.

(18) Lightfoot, P. D.; Roussel, P.; Veyret, B.; Lesclaux, R. *J. Chem. Soc. Faraday Trans.* **1990**, *86*, 2927.

(19) Jafri, J. A.; Phillips, D. H. *J. Am. Chem. Soc.* **1990**, *112*, 2586.

(20) Nielsen, O. J.; Wallington, T. J. In *Peroxyl Radicals*; John Wiley and Sons: New York, 1997; Chapter 5.

(21) Pushkarsky, M. B.; Zalyubovsky, S. J.; Miller, T. A. *J. Chem. Phys.* **2000**, *112*, 10695.

(22) Rupper, P.; Sharp, E. N.; Tarczay, G.; Miller, T. A. *J. Phys. Chem. A* **2007**, *111*, 832.

(23) Zalyubovsky, S. J.; Glover, B. G.; Miller, T. A.; Hayes, C.; Merle, J. K.; Hadad, C. M. *J. Phys. Chem. A* **2005**, *109*, 1308.

(24) Glover, B. G.; Miller, T. A. *J. Phys. Chem. A* **2005**, *109*, 11191.

(25) Tarczay, G.; Zalyubovsky, S. J.; Miller, T. A. *Chem. Phys. Lett.* **2005**, *406*, 81.

(26) Rothman, L. S.; Jacquemart, D.; Barbe, A.; Benner, D. C.; Birk, M.; Brown, L. R.; Carleer, M. R.; Chackerian, J. C.; Chance, K.; Coudert, L. H.; Dana, V.; Devi, V. M.; Flaud, J.-M.; Gamache, R. R.; Goldman, A.; Hartmann, J.-M.; Jucks, K. W.; Maki, A. G.; Mandin, J.-Y.; Massie, S. T.; Orphal, J.; Perrin, A.; Rinsland, C. P.; Smith, M. A. H.; Tennyson, J.; Tolchenov, R. N.; Toth, R. A.; Auwera, J. V.; Varanasi, P.; Wagner, G. *J. Quant. Spectrosc. Radiat. Transfer* **2005**, *96*, 139.

(27) Ahmed, M.; Blunt, D.; Chen, D.; Suits, A. G. *J. Chem. Phys.* **1997**, *106*, 7617.

(28) Baklanov, A. V.; Krasnoperov, L. N. *J. Phys. Chem. A* **2001**, *105*, 97.

(29) Bennett, J. G.; Bunce, S. C. *J. Org. Chem.* **1960**, *25*, 73.

(30) Stanton, J. F.; Gauss, J. *J. Chem. Phys.* **1994**, *101*, 8938.

(31) Dunning, T. H.; Hay, P. J. In *Methods of Electronic Structure Theory Vol. 2*; Plenum Press: New York, 1977.

(32) Frisch, M. J.; Trucks, G. W.; Schlegel, H. B.; Scuseria, G. E.; Robb, M. A.; Cheeseman, J. R.; Montgomery, J. A., Jr.; Vreven, T.; Kudin, K. N.; Burant, J. C.; Millam, J. M.; Iyengar, S. S.; Tomasi, J.; Barone, V.; Mennucci, B.; Cossi, M.; Scalmani, G.; Rega, N.; Petersson, G. A.; Nakatsuji, H.; Hada, M.; Ehara, M.; Toyota, K.; Fukuda, R.; Hasegawa, J.; Ishida, M.; Nakajima, T.; Honda, Y.; Kitao, O.; Nakai, H.; Klene, M.; Li, X.; Knox, J. E.; Hratchian, H. P.; Cross, J. B.; Bakken, V.; Adamo, C.; Jaramillo, J.; Gomperts, R.; Stratmann, R. E.; Yazyev, O.; Austin, A. J.; Cammi, R.; Pomelli, C.; Ochterski, J. W.; Ayala, P. Y.; Morokuma, K.; Voth, G. A.; Salvador, P.; Dannenberg, J. J.; Zakrzewski, V. G.; Dapprich, S.; Daniels, A. D.; Strain, M. C.; Farkas, O.; Malick, D. K.; Rabuck, A. D.; Raghavachari, K.; Foresman, J. B.; Ortiz, J. V.; Cui, Q.; Baboul, A. G.; Clifford, S.; Cioslowski, J.; Stefanov, B. B.; Liu, G.; Liashenko, A.; Piskorz, P.; Komaromi, I.; Martin, R. L.; Fox, D. J.; Keith, T.; Al-Laham, M. A.; Peng, C. Y.; Nanayakkara, A.; Challacombe, M.; Gill, P. M. W.; Johnson, B.; Chen, W.; Wong, M. W.; Gonzalez, C.; Pople, J. A. *Gaussian 03*, revision C.02; Gaussian, Inc.: Wallingford, CT, 2004.

(33) Gaussview, Version 3.09. Dennington, R., II; Keith, T.; Millam, J.; Eppinnett, K.; Hovell, W. L.; Gilliland, R.

(34) Just, G. M. P.; McCoy, A. B.; Miller, T. A. *J. Chem. Phys.* **2007**, *127*, 044310.

(35) Sharp, E. N.; Rupper, P.; Miller, T. A. *Phys. Chem. Chem. Phys.* invited review, submitted.

(36) Herzberg, G. In *Molecular Spectra and Molecular Structure Vol. II*; Krieger: Malabar, 1991; chapter Infrared and Raman Spectra of Polyatomic Molecules.